Jumping-Droplet Electrostatic Energy Harvesting

Nenad Miljkovic,[1] Daniel J. Preston,[1] Ryan Enright,[2] and Evelyn N. Wang[1,*]

[1]*Department of Mechanical Engineering, Massachusetts Institute of Technology, 77 Massachusetts Avenue, Cambridge, Massachusetts 02139, USA*
[2]*Thermal Management Research Group, Efficient Energy Transfer (ηET) Department, Bell Labs Ireland, Alcatel-Lucent Ireland Ltd., Blanchardstown Business & Technology Park, Snugborough Rd, Dublin 15, Ireland*

*Address correspondence to enwang@mit.edu

Abstract

Micro- and nanoscale wetting phenomena has been an active area of research due to its potential for improving engineered system performance involving phase change. With the recent advancements in micro/nanofabrication techniques, structured surfaces can now be designed to allow condensing coalesced droplets to spontaneously jump off the surface due to the conversion of excess surface energy into kinetic energy. In addition to being removed at micrometric length scales (~10 μm), jumping water droplets also attain a positive electrostatic charge (~10 - 100 fC) from the hydrophobic coating/condensate interaction. In this work, we take advantage of this droplet charging to demonstrate jumping-droplet electrostatic energy harvesting. The charged droplets jump between superhydrophobic copper oxide and hydrophilic copper surfaces to create an electrostatic potential and generate power during formation of atmospheric dew. We demonstrated power densities of ~15 pW/cm^2, which, in the near term, can be improved to ~1 μW/cm^2. This work demonstrates a surface engineered platform that promises to be low cost and scalable for atmospheric energy harvesting and electric power generation.

KEYWORDS: energy harvesting, electrostatic generator, condensation, jumping droplet, superhydrophobic, nanostructured, droplet charging

Energy harvesting or 'energy scavenging' is the conversion of ambient energy present in the environment into electrical energy.[1-4] Typically, energy harvesting involves the conversion of small amounts of ambient energy to power small (~1 cm), low-power (~1 μW) electronic devices. Ambient energy sources suitable for harvesting include: light,[5] heat,[6] vibration,[1,7,8] movement,[9] radio waves,[10] electromagnetic (EM) fields,[11] and airflow[12]. In addition to being pollution free, the harvested energy is usually derived from waste energy streams that are otherwise not harnessed for useful work. Energy harvesting has therefore attracted much interest because of its potential use as a power supply in applications such as low-power wireless sensor networks[13] and electronic systems.[14]

In this work, we experimentally demonstrated jumping-droplet-based energy harvesting with nanoengineered superhydrophobic surfaces. Recent studies have shown that when small water droplets (~10 – 100 μm) merge on superhydrophobic nanostructured surfaces, droplets can spontaneously eject *via* the release of excess surface energy irrespective of gravity.[15,16] A number of works have since fabricated superhydrophobic nanostructured surfaces to achieve spontaneous droplet removal[17-20] for a variety of applications including self-cleaning,[21] condensation heat transfer enhancement,[22-28] thermal diodes,[29,30] and anti-icing.[31-33] Furthermore, we recently discovered that these jumping droplets are positively charged (~10 – 100 fC), due to electric-double-layer charge-separation at the hydrophobic coating/condensate interface,[34] and can be manipulated with electric fields.[24] Here, we take advantage of this unique droplet-charging phenomenon to demonstrate jumping-droplet energy harvesting, where the charged droplets jump between superhydrophobic copper oxide (CuO) and hydrophilic copper (Cu) surfaces to

create an electrostatic potential and generate power by direct condensation of atmospheric moisture. We experimentally demonstrated power densities of ~15 pW/cm^2 and describe near-term approaches to increase power densities to ~1 μW/cm^2.

To investigate jumping-droplet energy harvesting, we interdigitated nanostructured superhydrophobic CuO and hydrophilic Cu combs. The CuO nanostructures (Fig. 1a) were grown on commercially purchased Cu heat sinks (comb) with overall dimensions 26 x 89 x 75 mm (height x width x depth) (E1U-NPFSS-30, Cooler Master). Each comb had 14 fins which measured 18.7 mm and 0.48 mm in height and thickness, respectively. Alternating fins were removed to increase spacing during interdigitation and avoid short circuiting. Each comb was cleaned in an ultrasonic bath with acetone for 10 min and rinsed with ethanol, isopropyl alcohol and deionized (DI) water. The combs were then dipped into a 2.0-M hydrochloric acid solution for 10 min to remove the native oxide film on the surface, then triple-rinsed with DI water and dried with clean nitrogen gas. Nanostructured CuO films were formed by immersing one of the cleaned combs into a hot (96±3°C) alkaline solution composed of $NaClO_2$, NaOH, Na_3PO_4•$12H_2O$ and DI water (3.75: 5: 10: 100 wt%).[35] During the oxidation process, a thin (≈300 nm) Cu_2O layer was formed that then re-oxidized to form sharp, knife-like CuO oxide structures with heights of $h \approx 1$ μm, a solid fraction $\varphi \approx 0.023$ and a roughness factor $r \approx 10$. To render the CuO coated comb superhydrophobic, a P2i hydrophobic coating (Fig. 1(b)) was applied with plasma-enhanced vapor deposition. This process allowed for the development of a highly conformal (≈30-nm thick) polymer layer that is covalently bonded with the CuO surface. Goniometric measurements (MCA-3, Kyowa Interface Science) of ≈100 nl droplets on a smooth P2i-coated silicon wafer surface showed advancing and receding contact angles of θ_a = 124.3°±3.1° and θ_r = 112.6°±2.8°, respectively. Meanwhile, the advancing and receding

contact angles on the superhydrophobic CuO surface were measured to be $\theta_{a,CuO}$ = 171°±3° and $\theta_{r,CuO}$ = 164°±4°, respectively.

To harvest energy from the charged jumping droplets, the temperature of the CuO comb was reduced *via* a cooling water flow (Fig. 2) until jumping-droplet-condensation occurred. To visualize the behavior, the interdigitated device was tested in a controlled condensation chamber interfaced with a high speed camera.[36] Due to electric-double-layer charge separation at the liquid-hydrophobic coating interface,[34] the jumping droplets departed the surface with a droplet radius dependent electrostatic charge (≈10-100 fC). The jumping droplets travelled from the CuO comb fins and to the Cu hydrophilic comb fins (Movies 1-3),[36] resulting in an electric potential buildup by charge accumulation (Fig. 2(c)). Along the droplet trajectory, the electric field between the fins and viscous drag decelerated the jumping droplets. As the droplets moved to a location of higher potential (hydrophilic fins), their kinetic energy was directly converted into electrical energy, analogous to electrostatic energy generation.[37,38] Current was drawn from the high potential hydrophilic fin to do useful work.

To measure the electrostatic power generation of the interdigitated device, we measured the open circuit voltage (V_{OC}) and short circuit current (I_{SC}) between the two combs during condensation using a Keithley 6517B Electrometer. The high accuracy electrometer was connected to the interdigitated combs *via* an electrical feed through on the chamber. The chamber and electrometer chassis were grounded to the optical table beneath them. The chamber acted as both a ground and a shield for the electrical measurements. (For more details on the experimental setup and procedures, see sections S.2 and S.3 of the supplementary materials.[36])

To replicate atmospheric dew conditions, the energy harvesting process was studied at a cooling water temperature of $T_c \approx 8$°C and water vapor pressure of $P_v \approx 2$ kPa.[39] Figures 3(a) and

(b) show the independently measured V_{OC} and I_{SC} of the device, respectively. The V_{OC} was obtained by connecting the positive terminal of the electrometer to the Cu comb, and the negative terminal to the CuO comb and measuring the voltage potential during condensation. The I_{SC} was obtained by electrically connecting the Cu and CuO combs in series through the electrometer and measuring the current during condensation (For electrical circuit diagrams, see Fig. S4 of the supplementary material.[36]). Prior to condensation, V_{OC} and I_{SC} were ≈0 (t < 16 minutes in Fig. 3b). To initiate the condensation process for the electrical measurements, the cooling water temperature was decreased (t ≈ 16 minutes in Fig. 3b) until jumping droplet condensation was observed between the fins of the interdigitated device (Movies 1-3).[36] During condensation, the vapor pressure (P_v) decreased due to the finite amount of vapor inside the chamber and T_c was maintained ≈7.1 ± 0.5°C. As the condensation process intensified due to transient cooling of the CuO fins, V_{OC} and I_{SC} increased and eventually reached quasi-steady values of V_{OC} ≈ 15 V, and I_{SC} ≈ 1.15 nA, respectively (t ≈ 17.5 minutes in Fig. 3b). After ≈ 30 seconds of reaching a steady measurement, the cooling water temperature was increased (t ≈ 18 minutes in Fig. 3b) and V_{OC} and I_{SC} slowly decayed with time due to the smaller supersaturation for condensation, and lower droplet jumping frequency. The maximum energy-harvesting rate in these experiments was approximated by $P_{MAX} = 0.25 I_{SC} V_{OC}$ ≈ 15 pW/cm^2, whereby the prefactor of 0.25 accounts for a balanced resistive load being powered by the generator. The relatively low energy density of our device was mainly due to: i) the low cooling rates (<0.01 W/cm^2), and ii) the non-optimum fin arrangement, resulting in the coldest temperature being at the base of the superhydrophobic fins (due to cooling at the base) and the inability to maximize the use of the whole comb area for droplet jumping.

To provide insight into the experimental results, and estimate the maximum potential of jumping-droplet energy harvesting, we developed a model to determine V_{OC} and I_{SC} based on the heat transfer during condensation. Assuming a jumping-droplet radius of $R \approx 10$ μm,[22] and relating the condensation heat flux (q") to the energy associated with the latent heat of phase change per droplet ($\rho V h_{fg}$), the frequency of jumping droplets leaving the superhydrophobic surface per unit area (f) can be determined explicitly as $f = q"/(V h_{fg} \rho)$, where V and ρ are the jumping-droplet volume ($(4/3)\pi R^3$) and density (≈1000 kg/m^3), respectively. Assuming that all of the departing droplets leave the superhydrophobic surface and reach the hydrophilic surface, the short circuit current per unit area can be calculated from $I_{SC} = f Q_d$, where Q_d is the individual droplet charge ($Q_d \approx 8$ fC for $R \approx 10$ μm).[34] By considering the parallel CuO and Cu surfaces as capacitors with a separation distance d, the open circuit voltage can be determined by considering the case when charged jumping droplets will only be able to reach the hydrophilic fin with the kinetic energy available. At the open circuit condition, the droplets are decelerated along their trajectory by the force exerted by the electric field E on the droplet charge Q_d, with the force balance $ma = -Q_d E - F_{fr}$, where F_{fr} is the drag force due to the surrounding gas phase. To estimate an upper limit of V_{OC}, we assumed the drag force to be zero. Balancing the total jumping-droplet kinetic energy ($E_d = (1/2)\rho V u^2$) with the work required to traverse the electric field ($W_d = Q_d E d$), we obtained $V_{OC} = (\rho V u^2)/(2Q_d)$. Therefore, the maximum theoretical device power per unit area is approximated as $P_{MAX} = 0.25 I_{SC} V_{OC}$ for a balanced load. Explicitly, P_{MAX} can be re-written in terms of the experimental parameters as:

$$P_{MAX} = \frac{q" u^2}{8 h_{fg}}, \quad (1)$$

Equation (1) suggests that the most important parameter for further increasing the energy harvesting power generation is to increase the jumping-droplet velocity ($P_{MAX} \sim u^2$) by minimizing the jumping-droplet radius. For the simplest case of two, equally-sized inviscid spherical droplets coalescing on a surface with no adhesion, the energy-balance gives a characteristic jumping speed that follows an inertial-capillary scaling $u \sim \sqrt{\gamma/\rho R}$, where γ is the droplet surface tension.[15,16] Previous condensation experiments on these superhydrophobic CuO surfaces have shown that jumping water droplets with radii approaching ≈10 μm had a maximum jumping velocity of ≈1 m/s.[16,24] However, limited approaches exist to attain further increases in jumping-droplet velocity other than minimizing the surface droplet adhesion[16] and droplet departure diameter. A secondary and more practical approach to increase the energy harvesting rate is to maximize the condensation heat flux ($P_{MAX} \sim q''$) and jumping-droplet frequency in order to attain energy harvesting values approaching ~μW/cm^2 (Fig. 4).

The electrostatic energy harvesting method demonstrated here is similar to but fundamentally different from the Kelvin water droplet generator.[40] In the Kelvin generator, gravity opposes the electrostatic force acting on the droplets, whereas in our device, inertia of the jumping droplets opposes the electrostatic force. The main advantage of our jumping droplet approach stems from the reduced droplet size (R < 50 μm) and higher charge densities ($Q_d/(\rho V)$) obtainable with microdroplets.[41] More recently, researchers have demonstrated highly-efficient 'ballistic' electrostatic generation using charged microdroplets pumped through a micropore directed at a target conductor.[37] The fundamental principles of operation demonstrated with 'ballistic' and jumping-droplet generation are identical in nature (inertia opposes the electrostatic force). However, jumping-droplet electrostatic generation offers three main advantages: 1) it allows passive energy harvesting from the atmosphere *via* the formation

of dew, 2) the lack of moving parts and requirement for pumping to create a microjet make it passive and simpler in design, and 3) it utilizes low quality thermal energy (condensation) instead of high quality mechanical energy (pressure) to generate power.

This work demonstrates that jumping-droplet condensation can be used for electrostatic energy harvesting. In the future, it would be interesting to investigate the performance of the device under different load resistances. The use of variable load resistances will change the potential build-up in the device, and alter the overall device performance. In addition, the fabrication of high surface area devices promises to further increase the energy density of the energy harvesting, in addition to reducing the environmental footprint. Furthermore, the inclusion of frictional drag and other associated energy dissipation mechanisms into the theoretical calculations will provide insights to further improve device design by identifying additional critical parameters (*i.e.*, surrounding gas density and viscosity) to maximize power output.

In summary, we demonstrated jumping-droplet electrostatic energy harvesting, whereby charged droplets jump between superhydrophobic copper oxide and hydrophilic copper surfaces to create an electric potential and generate power during formation of atmospheric dew. Through experiments and modeling, we demonstrated power densities of ~15 pW/cm^2, which can be improved in the near-term to ~1 $\mu W/cm^2$. Future devices with higher condensation rates (>1 W/cm^2) and high-surface-area designs have the potential to achieve energy harvesting rates, making them more attractive to power small electronic devices (>1 μW, *i.e.*, chemical batteries, thermoelectrics, and piezoelectrics).[42,43] This work demonstrates a surface engineered platform that promises to be low cost and scalable for atmospheric energy harvesting and electrostatic power generation.

Acknowledgements

We thank Professor Borivoje B. Mikic of MIT for fruitful discussions regarding jumping-droplet power generation. We gratefully acknowledge funding support from the MIT S3TEC Center, an Energy Frontier Research Center funded by the Department of Energy, Office of Science, Basic Energy Sciences under Award # DE-FG02-09ER46577, and the Office of Naval Research (ONR) with Dr. Mark Spector as program manager. D.J.P. acknowledges funding received by the National Science Foundation Graduate Research Fellowship under Grant No. 1122374. Any opinion, findings, and conclusions or recommendations expressed in this material are those of the authors(s) and do not necessarily reflect the views of the National Science Foundation. R.E. acknowledges funding received from the Irish Research Council for Science, Engineering, and Technology, cofunded by Marie Curie Actions under FP7. Bell Labs Ireland thanks the Industrial Development Agency (IDA) Ireland for their financial support. We acknowledge support from P2i for the hydrophobic layer depositions. We also acknowledge the support from the National Science Foundation through the Major Research Instrumentation Grant for Rapid Response Research (MRI-RAPID) for the microgoniometer.

References:

[1]S. P. Beeby, M. J. Tudor, and N. M. White, Meas Sci Technol **17** (12), R175 (2006).
[2]D. B. Zhu, M. J. Tudor, and S. P. Beeby, Meas Sci Technol **21** (2) (2010).
[3]J. W. Matiko, N. J. Grabham, S. P. Beeby, and M. J. Tudor, Meas Sci Technol **25** (1) (2014).
[4]S. Priya and D. J. Inman, *Energy harvesting technologies*. (Springer, New York, 2009).
[5]B. Oregan and M. Gratzel, Nature **353** (6346), 737 (1991).
[6]F. J. DiSalvo, Science **285** (5428), 703 (1999).
[7]S. R. Anton and H. A. Sodano, Smart Mater Struct **16** (3), R1 (2007).
[8]J. K. Moon, J. Jeong, D. Lee, and H. K. Pak, Nature Communications **4** (2013).
[9]P. D. Mitcheson, E. M. Yeatman, G. K. Rao, A. S. Holmes, and T. C. Green, P Ieee **96** (9), 1457 (2008).
[10]A. M. Hawkes, A. R. Katko, and S. A. Cummer, Appl Phys Lett **103** (16) (2013).
[11]S. Kulkarni, E. Koukharenko, J. Tudor, S. Beeby, T. O'Donnell, and S. Roy, Transducers '07 & Eurosensors Xxi, Digest of Technical Papers, Vols 1 and 2, U444 (2007).
[12]D. B. Zhu, S. P. Beeby, M. J. Tudor, N. M. White, and N. R. Harris, Ieee Sens J **13** (2), 691 (2013).
[13]Y. K. Tan and S. K. Panda, Ieee T Instrum Meas **60** (4), 1367 (2011).
[14]J. Ortiz, P. M. Monje, G. Aranguren, S. Corbo, V. Cokonaj, E. Barrera, and M. Ruiz, Structural Health Monitoring 2013, Vols 1 and 2, 1597 (2013).
[15]J. B. Boreyko and C. H. Chen, Phys Rev Lett **103** (18), 184501 (2009).
[16]R. Enright, N. Miljkovic, J. Sprittles, R. Mitchell, K. Nolan, and E. N. Wang, in review (2014).
[17]X. M. Chen, J. Wu, R. Y. Ma, M. Hua, N. Koratkar, S. H. Yao, and Z. K. Wang, Advanced Functional Materials **21** (24), 4617 (2011).
[18]K. Rykaczewski, A. T. Paxson, S. Anand, X. Chen, Z. Wang, and K. K. Varanasi, Langmuir **29** (3), 881 (2013).
[19]J. Feng, Z. Q. Qin, and S. H. Yao, Langmuir **28** (14), 6067 (2012).
[20]N. Miljkovic, D. J. Preston, R. Enright, S. Adera, Y. Nam, and E. N. Wang, Journal of Heat Transfer **135** (8), 080907 (2013).
[21]K. M. Wisdom, J. A. Watson, X. P. Qu, F. J. Liu, G. S. Watson, and C. H. Chen, Proceedings of the National Academy of Sciences of the United States of America **110** (20), 7992 (2013).
[22]N. Miljkovic, R. Enright, Y. Nam, K. Lopez, N. Dou, J. Sack, and E. N. Wang, Nano Letters **13** (1), 179 (2013).
[23]N. Miljkovic, R. Enright, and E.N. Wang, Acs Nano **6** (2), 1776 (2012).
[24]N. Miljkovic, D. J. Preston, R. Enright, and E. N. Wang, ACS Nano **7** (12), 11043 (2013).
[25]N. Miljkovic and E. N. Wang, Mrs Bull **38** (5), 397 (2013).
[26]C. Dietz, K. Rykaczewski, A. G. Fedorov, and Y. Joshi, Appl Phys Lett **97** (3), 033104 (2010).
[27]R. Enright, N. Miljkovic, J. L. Alvarado, K. J. Kim, and J. W. Rose, Nanoscale and Microscale Thermophysical Engineering, in press (2014).
[28]R. Enright, N. Miljkovic, N. Dou, Y. Nam, and E. N. Wang, Journal of Heat Transfer **135** (9), 091304 (2013).
[29]J. B. Boreyko and C. H. Chen, Int J Heat Mass Tran **61**, 409 (2013).
[30]J. B. Boreyko, Y. J. Zhao, and C. H. Chen, Appl Phys Lett **99** (23), 234105 (2011).
[31]J. B. Boreyko and P. C. Collier, Acs Nano **7** (2), 1618 (2013).

[32]X. M. Chen, R. Y. Ma, H. B. Zhou, X. F. Zhou, L. F. Che, S. H. Yao, and Z. K. Wang, Sci Rep-Uk **3**, 2515 (2013).
[33]Q. L. Zhang, M. He, J. Chen, J. J. Wang, Y. L. Song, and L. Jiang, Chemical Communications **49** (40), 4516 (2013).
[34]N. Miljkovic, D. J. Preston, R. Enright, and E. N. Wang, Nature Communications **4**, 2517 (2013).
[35]Y. Nam and Y. S. Ju, Journal of Adhesion Science and Technology **27** (20), 2163 (2013).
[36]See supplemental material at APL website for high speed movies and detailed description of the experimental setup and procedures.
[37]Y. Xie, D. Bos, L. J. de Vreede, H. L. de Boer, M.-J. van der Meulen, M. Versluis, A. J. Sprenkels, A. van den Berg, and J. C. T. Eijkel, Nature Communications **5** (3575) (2014).
[38]N. Tesla, Scientific American **150**, 132 (1934).
[39]J. L. Monteith, Q J Roy Meteor Soc **83** (357), 322 (1957).
[40]W. Thomson, Proceedings of the Royal Society of London **16**, 391 (1867).
[41]A. G. Marin, W. van Hoeve, P. Garcia-Sanchez, L. L. Shui, Y. B. Xie, M. A. Fontelos, J. C. T. Eijkel, A. van den Berg, and D. Lohse, Lab Chip **13** (23), 4503 (2013).
[42]Z. L. Wang, *Nanogenerators for Self-Powered Devices and Systems*, SMARTech digital repository, Georgia Institute of Technology, 2011.
[43]Z. L. Wang and W. Wu, Angewandte Chemie International Edition **51**, 2 (2012).

FIGURES

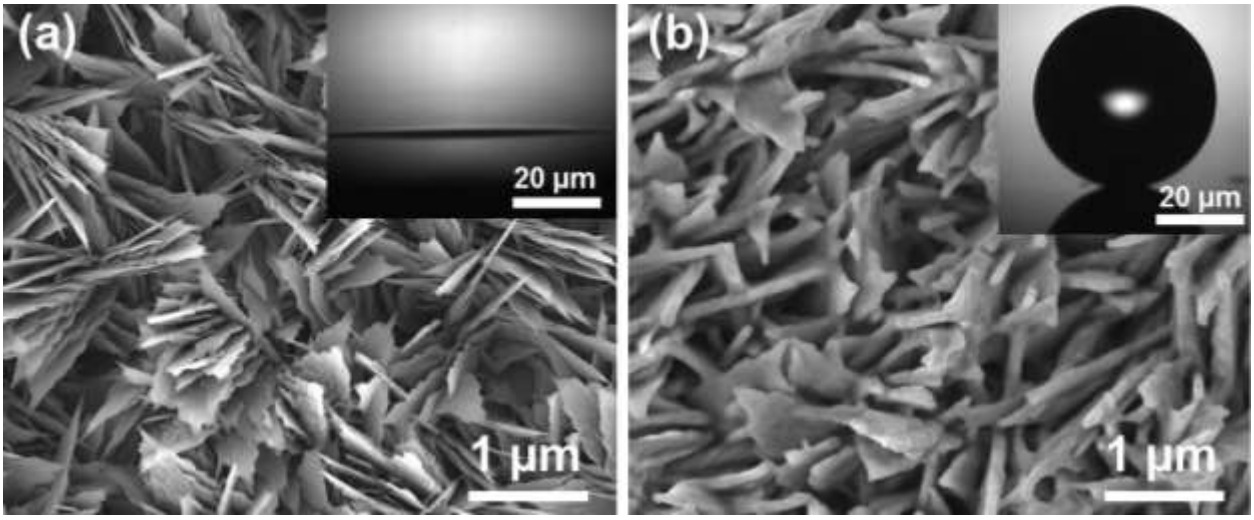

FIG. 1. (Single Column, AR = 2.45)

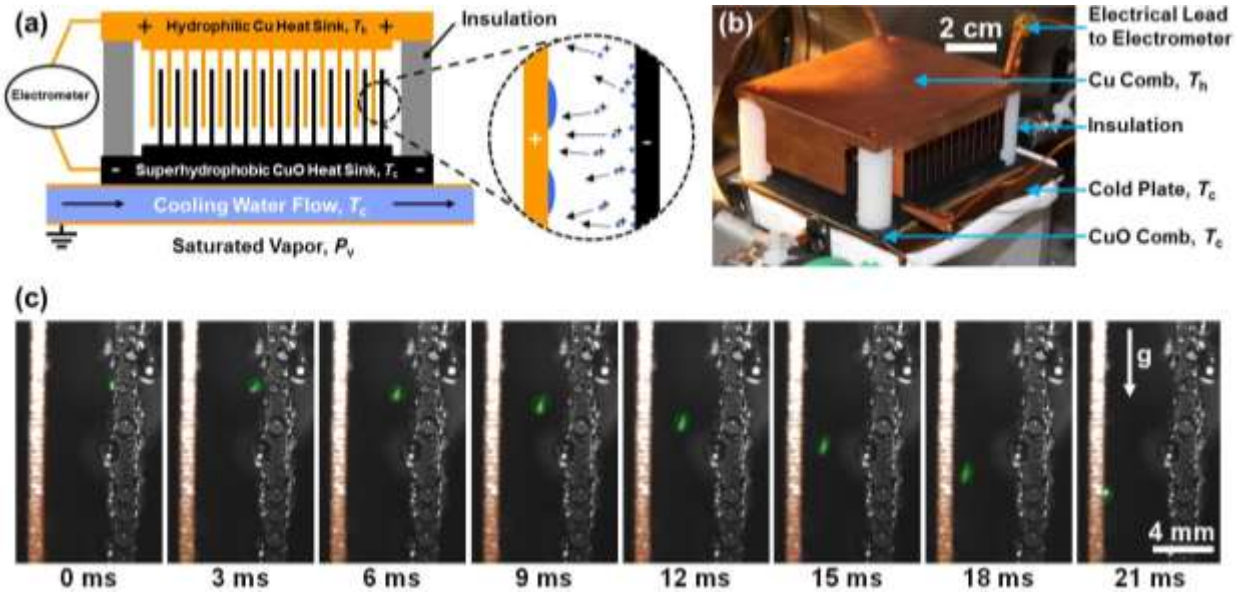

FIG. 2. (Double Column, AR = 2.12)

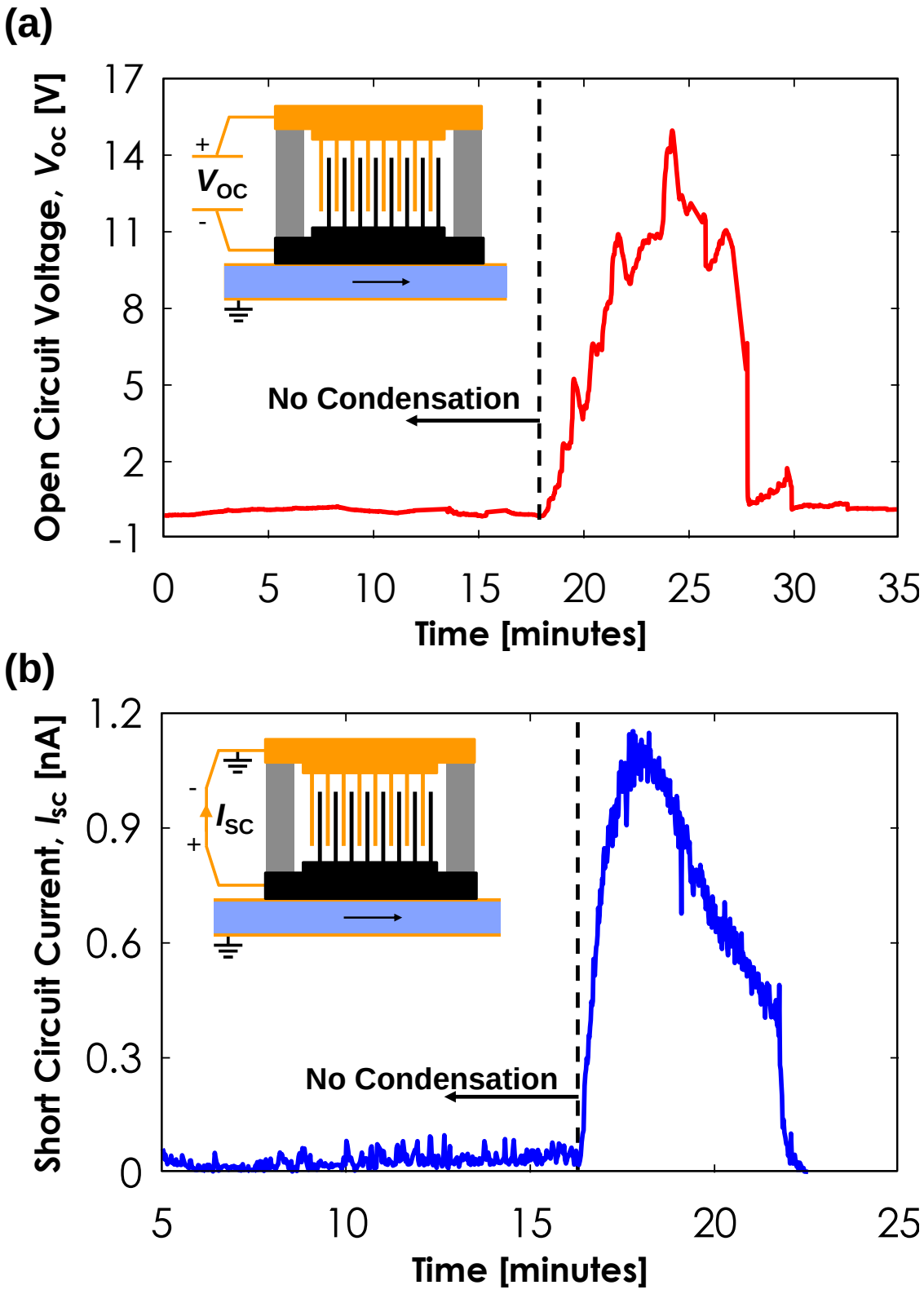

FIG. 3. (Single Column, AR = 0.75)

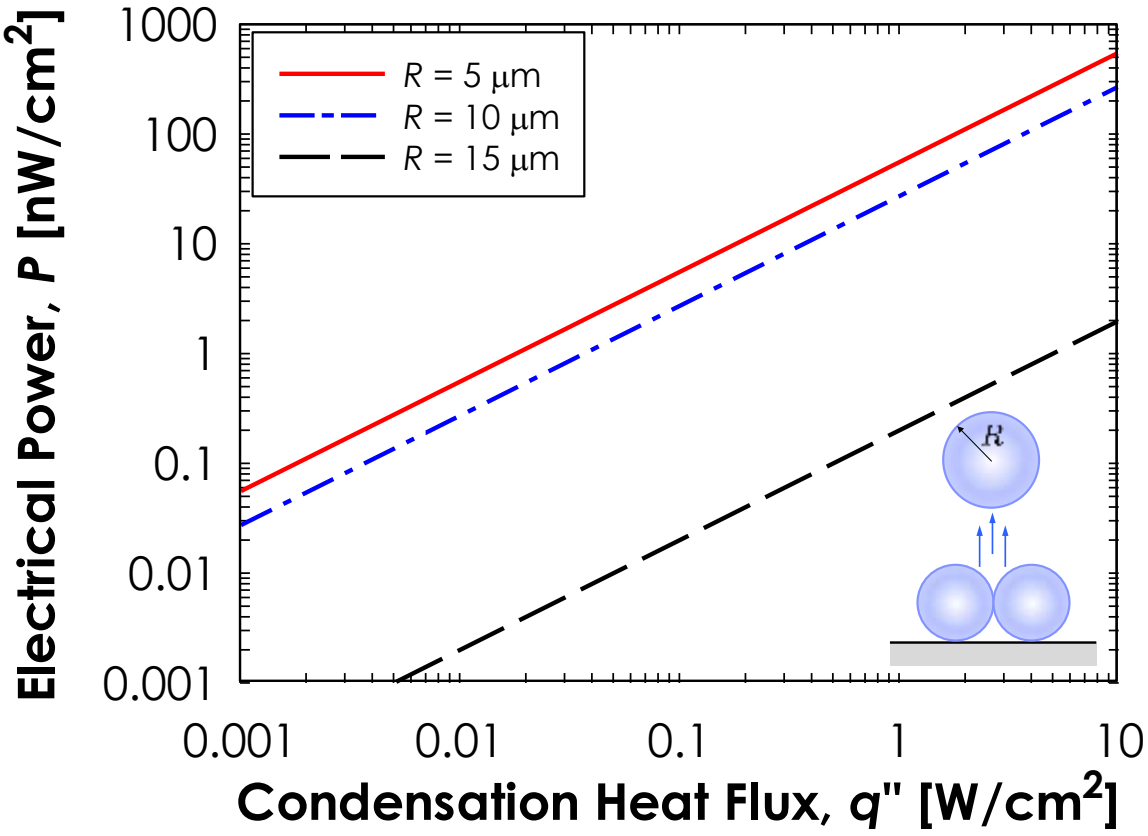

FIG. 4. (Single Column, AR = 1.34)

Figure and table legends

FIG 1. Field emission scanning electron micrographs (FESEM) of (a) a 10 minute oxidized CuO surface (Inset: Water droplet contact angle on the clean nanostructured CuO surface, $\theta_a \approx 0°$) and (b) a CuO surface coated with an ≈30 nm thick layer of P2i fluoropolymer (Inset: Water droplet advancing contact angle on the superhydrophobic nanostructured surface, $\theta_a = 171° \pm 3°$).

FIG 2. (a) Schematic of the jumping-droplet energy harvesting device showing the two combs in an interdigitated arrangement. The combs were electrically and thermally isolated from each other. Images of the jumping-droplet electrostatic generator showing (b) an isometric view of the two combs integrated in the test chamber for experimentation. Commercially purchased Cu combs were used (478 copper) with overall dimensions 26 x 89 x 75 mm (height x width x depth) and fin thickness of 0.48 mm (E1U-NPFSS-30, Cooler Master). To observe droplet jumping, the interdigitated device was tested in a controlled condensation chamber. (c) False-color time-lapse images captured *via* high speed imaging of droplet jumping (green) from the superhydrophobic CuO comb fin to the hydrophilic Cu comb fin (orange). High speed movie recorded at 1000 frames per second (P_v = 2 ± 0.2 kPa, T_c = 8 ± 0.5°C). (For experimental setup/procedure details and movies, see supplementary material.[36])

FIG 3. Experimentally measured (a) open circuit voltage (V_{OC}) and (b) short circuit current (I_{SC}) of the interdigitated device. The maximum electrostatic energy harvesting rate in these experiments ($P_{MAX} = 0.25 V_{OC} I_{SC}$) was ≈4.3 nW or ≈15 pW/cm^2 (based on an approximated prototype active jumping area of 278 cm^2). The experiments were conducted by filling the controlled chamber with saturated water vapor and closing off the vapor inlet valve. Once pressure and temperature equilibrium was reached, the cooling water temperature (T_c) was gradually decreased and the water vapor began to condense. Due to the finite volume of water vapor in the chamber, the saturation pressure decreased as well, resulting in a corresponding decrease in droplet-jumping frequency, V_{OC} and I_{SC} (P_v = 2 ± 0.2 kPa, T_c = 8 ± 0.5°C).[36]

FIG 4. Theoretically calculated electrostatic energy harvesting rate from jumping-droplet condensation. By considering the parallel CuO and Cu surfaces as capacitors with a separation distance d, the open circuit voltage V_{OC} and short circuit current I_{SC} was calculated by considering the case when charged jumping droplets will only reach the hydrophilic fin with the kinetic energy available. From these results, the maximum theoretical device power per unit area can be approximated for a balanced resistive load as $P_{MAX} = 0.25 I_{SC} V_{OC}$. The results show that increasing the condensation heat flux (q'') and decreasing the jumping-droplet radius (R) increases the electrostatic power generation. This is due to the corresponding increase in jumping-droplet frequency (current) and larger jumping-droplet initial velocity (u). The model assumes a droplet departure velocity of 1, 0.7, and 0.6 m/s for droplet radii of 5, 10, and 15 μm, respectively.[16]

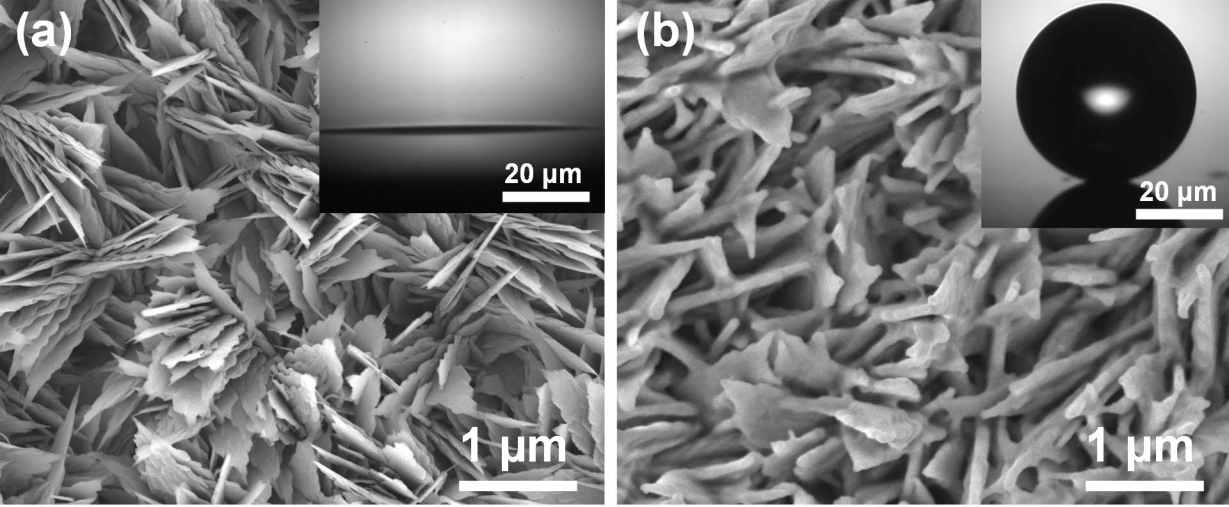
(a)
20 μm
1 μm
(b)
20 μm
1 μm

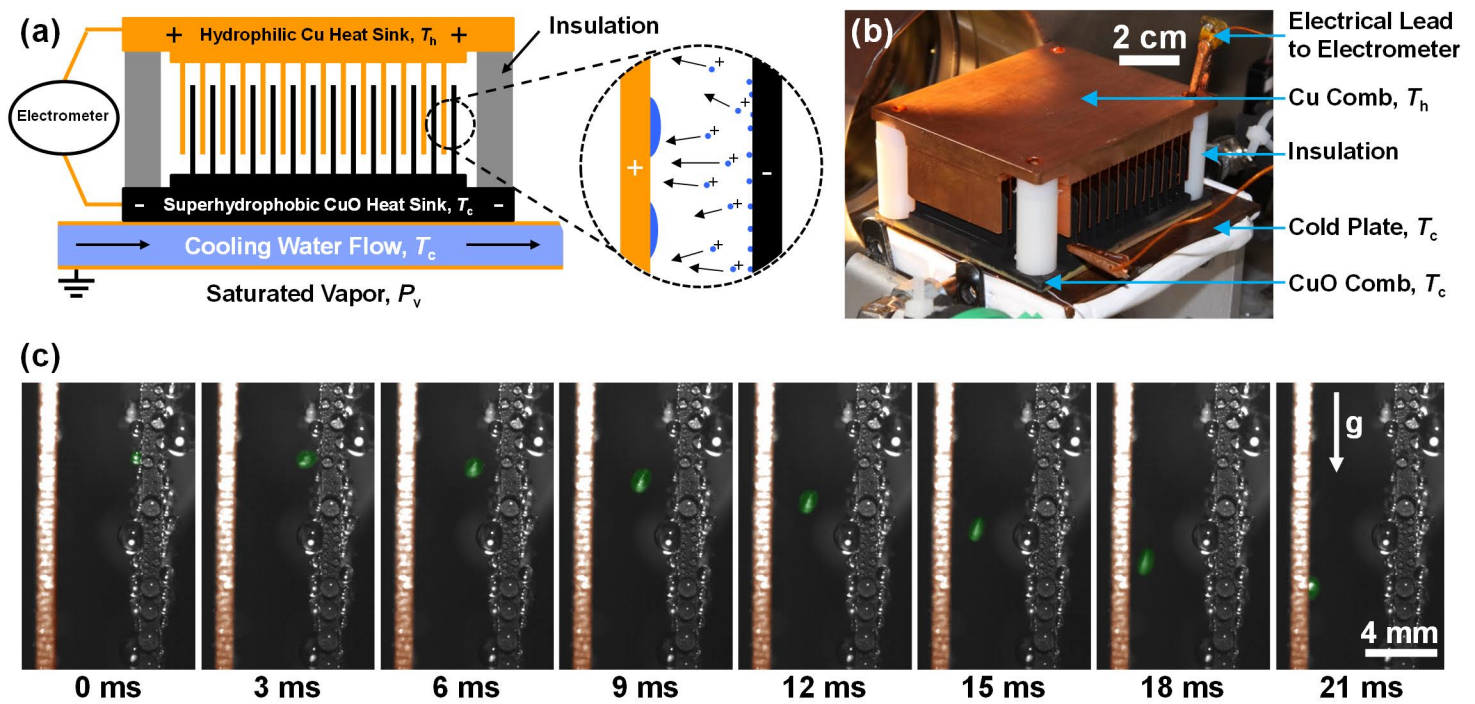
(a)
Hydrophilic Cu Heat Sink, T_h
Insulation
Electrometer
Superhydrophobic CuO Heat Sink, T_c
Cooling Water Flow, T_c
Saturated Vapor, P_v
(b)
2 cm
Electrical Lead to Electrometer
Cu Comb, T_h
Insulation
Cold Plate, T_c
CuO Comb, T_c
(c)
g
4 mm
0 ms
3 ms
6 ms
9 ms
12 ms
15 ms
18 ms
21 ms

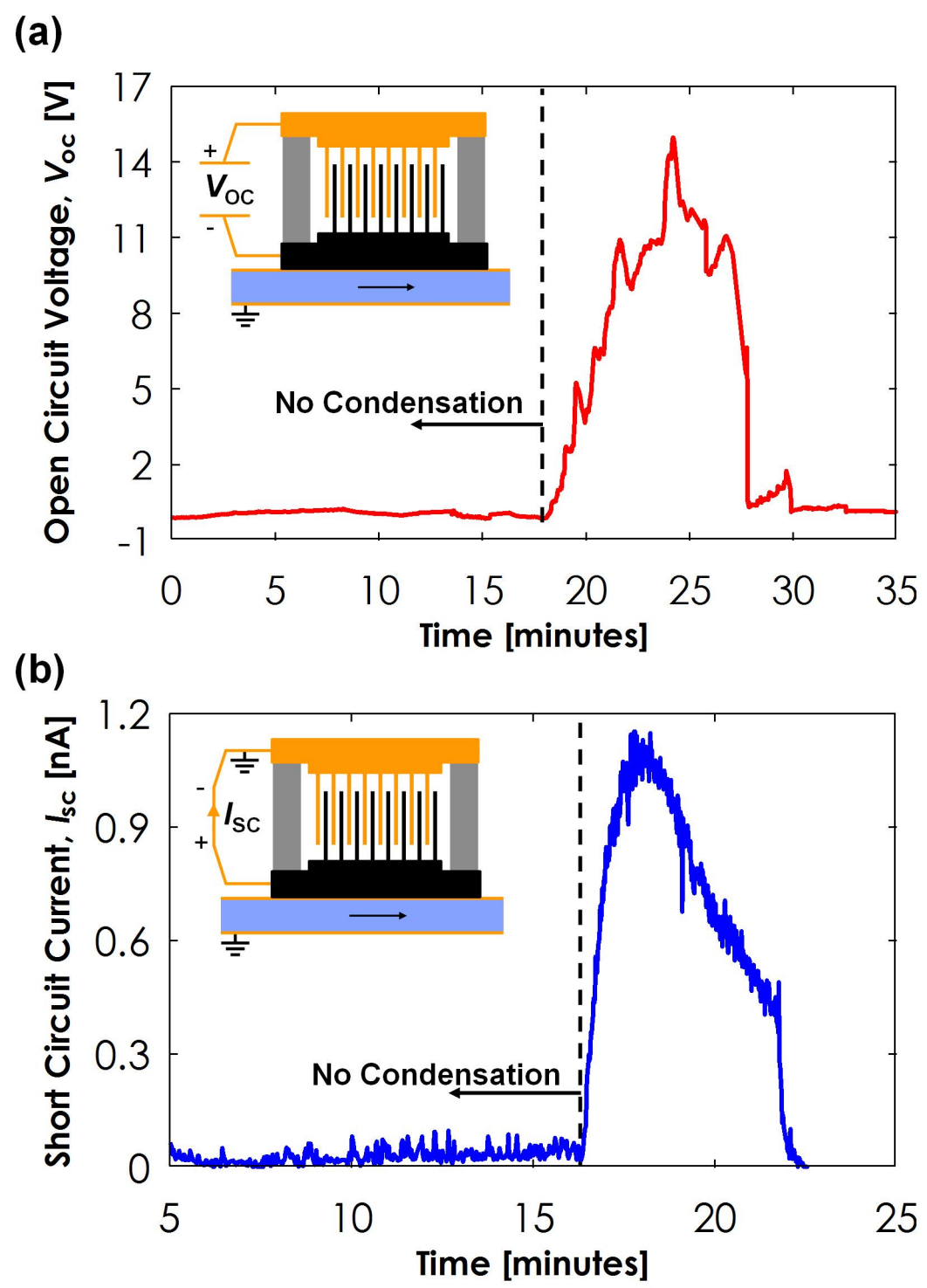
(a)
Open Circuit Voltage, V_{oc} [V]
17
14
11
8
5
2
-1
+
V_{OC}
-
No Condensation
0
5
10
15
20
25
30
35
Time [minutes]
(b)
Short Circuit Current, I_{sc} [nA]
1.2
0.9
0.6
0.3
0
-
I_{SC}
+
No Condensation
5
10
15
20
25
Time [minutes]

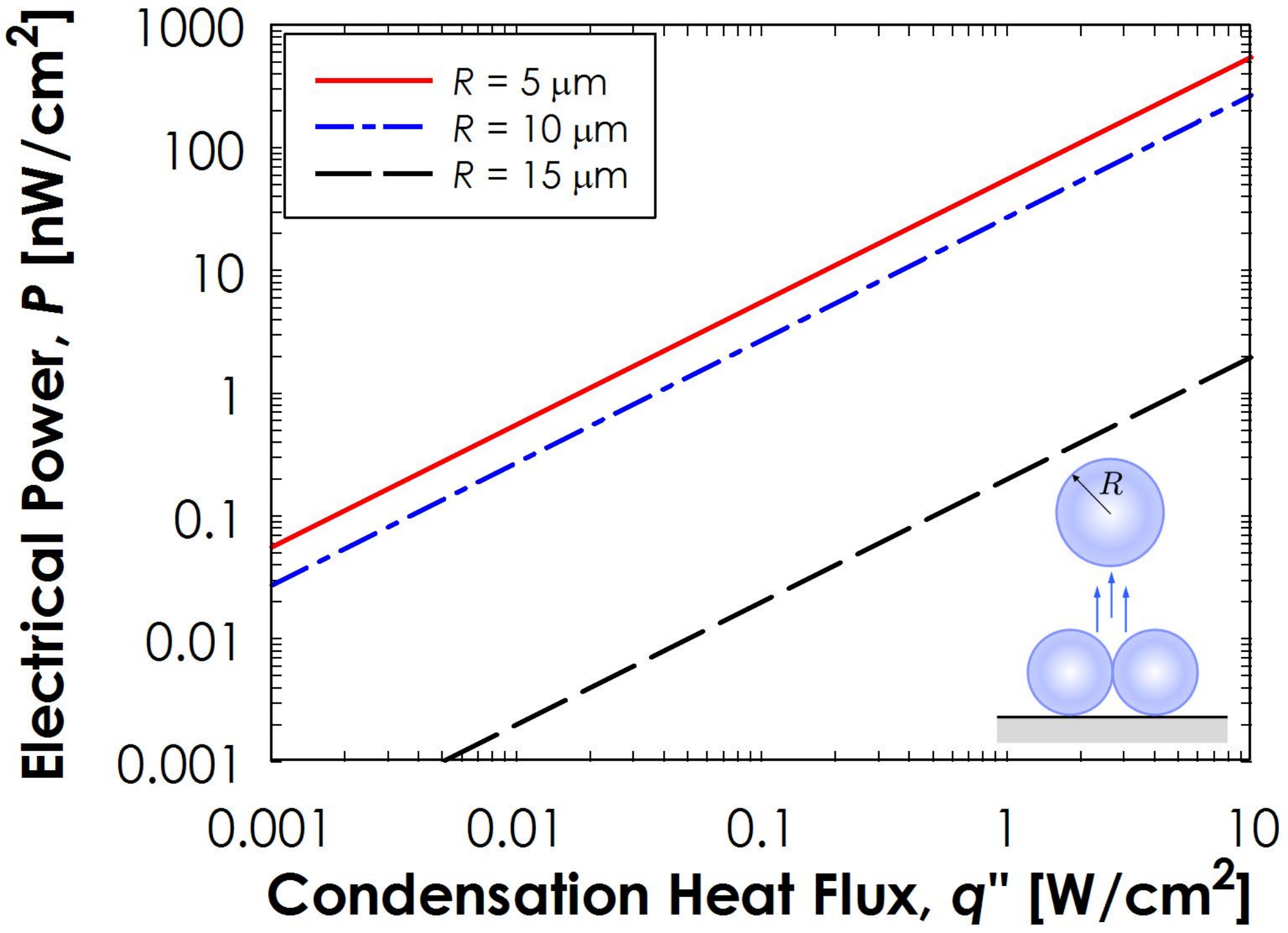
Electrical Power, P [nW/cm2]
1000
100
10
1
0.1
0.01
0.001
R = 5 μm
R = 10 μm
R = 15 μm
R
0.001
0.01
0.1
1
10
Condensation Heat Flux, q" [W/cm2]

Supplemental Material

Jumping-Droplet Electrostatic Energy Harvesting

Nenad Miljkovic,[1] Daniel J. Preston,[1] Ryan Enright,[2] and Evelyn N. Wang[1,*]

[1]*Department of Mechanical Engineering, Massachusetts Institute of Technology, 77 Massachusetts Avenue, Cambridge, Massachusetts 02139, USA*
[2]*Thermal Management Research Group, Efficient Energy Transfer (ηET) Department, Bell Labs Ireland, Alcatel-Lucent Ireland Ltd., Blanchardstown Business & Technology Park, Snugborough Rd, Dublin 15, Ireland*

*Address correspondence to enwang@mit.edu

S.1 HIGH SPEED MOVIES

Movies 1, 2, and 3. Droplet jumping during condensation and electrostatic power generation between superhydrophobic CuO (dark vertical fins) and hydrophilic Cu fins (bright vertical fins) captured with a high speed camera (Phantom v7.1, Vision Research). The fins were aligned by interdigitating Cu heat sinks (combs) with dimensions 26 x 89 x 75 mm (height x width x depth) (E1U-NPFSS-30, Cooler Master). The fin surfaces were oriented vertically (gravity facing downwards). Many small droplets jumped laterally from the CuO surfaces and landed on the adjacent Cu surfaces. Some jumping droplets reversed direction after jumping due to vapor flow entrainment and electrostatic repulsion and travelled back towards the CuO surface.[1] Once the returning droplets returned to the surface, they a) coalesced with other droplets on the surface and underwent a second jump,[2,3] or b) adhered to the CuO surface and grew *via* condensation until coalescing with a neighboring droplet and jumping from the surface again.[2] The vapor pressure was ≈1.8 kPa. The video was captured at 1000 fps and is played back at 20 fps. The field of view is 12.8 mm x 9.6 mm. Movie 2 corresponds to the false-color time-lapse images shown in Fig. 2(c) of the manuscript.

S.2 CONDENSATION CHAMBER SETUP

The custom environmental chamber used for this work (Kurt J. Lesker) consists of a stainless steel frame with a door (sealed with a rubber gasket), two viewing windows, and apertures for various components. Resistive heater lines were wrapped around the exterior of the chamber

walls to prevent condensation at the inside walls and then insulated on the exterior walls. The output power of the resistive heater lines was controlled by a voltage regulator (Variac). Two insulated stainless steel water flow lines (Swagelok) were fed into the chamber *via* a KF flange port (Kurt J. Lesker) to supply cooling water to the chamber from a large capacity chiller (System III, Neslab). The cooling water flow rate was measured *via* an in-line liquid flow meter (0-5 L/min L-Series liquid flow meter, Alicat)

A secondary stainless steel tube line was fed into the chamber *via* a KF adapter port that served as the flow line for the incoming water vapor supplied from a heated steel water reservoir. The vapor line was wrapped with a rope heater (60 W, Omega) and controlled by a power supply (Agilent). The vapor reservoir was wrapped with another independently-controlled rope heater (120 W, Omega) and insulated to limit heat losses to the environment. The access tubes were welded to the vapor reservoir, each with independently-controlled valves. The first valve (Diaphragm Type, Swagelok), connecting the bottom of the reservoir to the ambient, was used to fill the reservoir with water. The second valve (BK-60, Swagelok), connecting the top of the reservoir to the inside of the chamber, provided a path for vapor inflow. K-type thermocouples were located along the length of the water vapor reservoir to monitor temperature.

A bellows valve (Kurt J. Lesker) was attached to the chamber to serve as a leak port between the ambient and inside of the chamber. In order to monitor temperatures within the chamber, K-type thermocouple bundles were connected through the chamber apertures *via* a thermocouple feed through (Kurt J. Lesker). To provide electrical connections inside the chamber for LED lighting and electric field generation, insulated copper electrical wires were connected through the chamber apertures *via* an electrical feed through (Kurt J. Lesker). A pressure transducer (925 Micro Pirani, MKS) was attached to monitor pressure within the chamber. The thermocouple bundles and the pressure transducer were both electrically connected to an analog input source (RAQ DAQ, National Instruments), which was interfaced to a computer for data recording. A second bellows valve (Kurt J. Lesker) was integrated onto the chamber for the vacuum pump, which brought down the chamber to vacuum conditions prior to vapor filling. A liquid nitrogen cold trap was incorporated along the line from the chamber to the vacuum which served to remove any moisture from the pump-down process and ultimately assist in

yielding higher quality vacuum conditions. A tertiary bellows valve (Kurt J. Lesker) was integrated on a T fitting between the vacuum pump and liquid nitrogen reservoir to connect the vacuum line to the ambient to release the vacuum line to ambient conditions once pump down was achieved. In order to visually record data, a high speed camera (Phantom v7.1, Vision Research) was placed in line with the 5" viewing windows on the chamber. The schematic of the exterior of the environmental setup is depicted in Fig. S1(a). Images of the front and rear of the experimental setup are shown in Fig. S1(b) and Fig. S1(c), respectively.

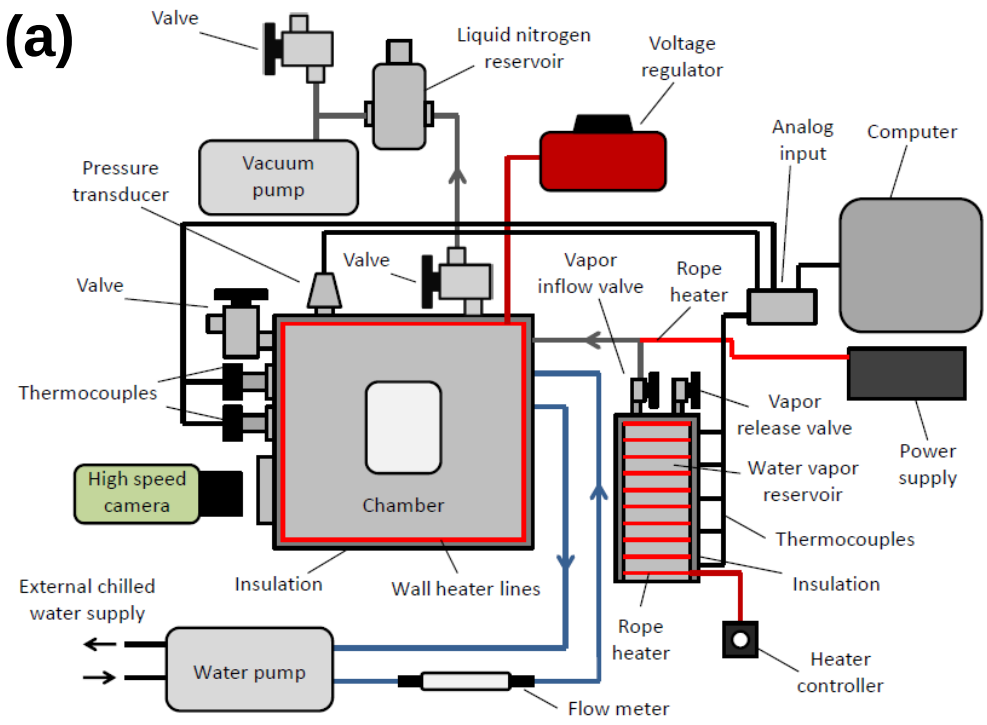

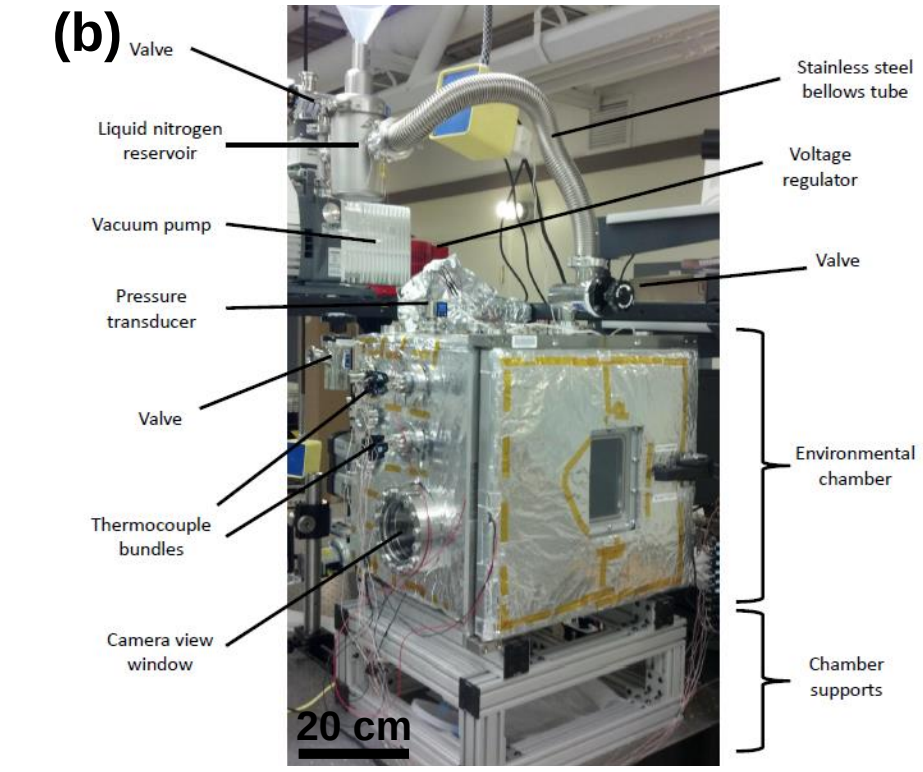

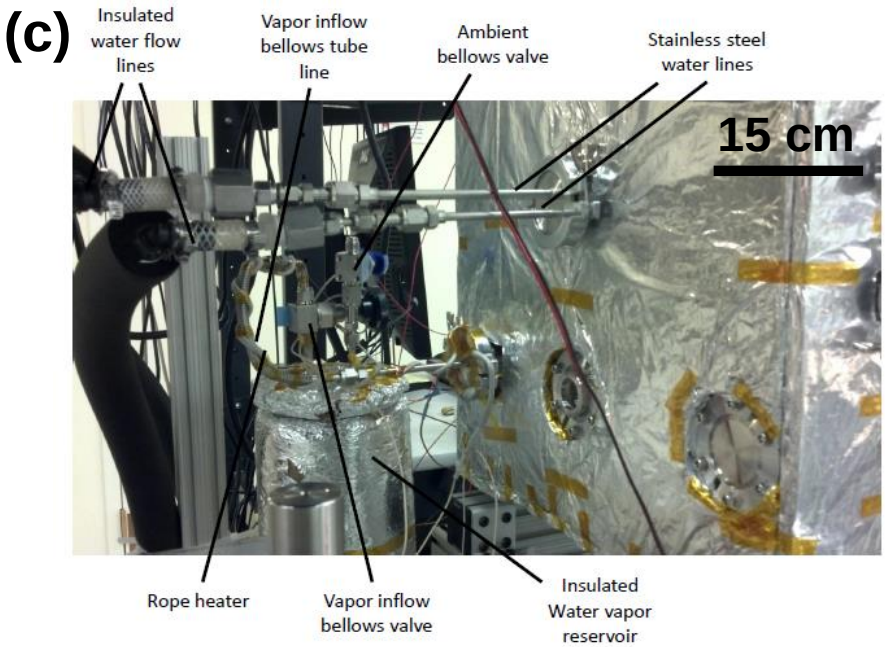

FIG. S1. (a) Schematic of experimental setup (not to scale). (b) Image of the experimental setup shown from the front (high speed camera and data acquisition system not shown). (c) Image of the experimental setup from the rear of the chamber showing the cooling water inlet and outlet and water vapor reservoir. Reprinted with permission from [4]. Copyright 2012 American Chemical Society.

The setup used to run experiments inside the chamber is shown in Fig S2. Stainless steel bellows tube lines (1/4”, Swagelok) were connected to the external water flow lines (Fig. S1(c)). T-connection adapters (Swagelok) with bore through Ultra-Torr fittings (Swagelok) were used to adapt K-type thermocouple probes (Omega) at the water inlet and outlet.

The interdigitated comb test platform consisted of a 10.1 x 8.7 x 0.49 cm custom made copper cold plate which was connected *via* a Swagelok compression fitting onto the T-connection. The cold plate was manufactured by bending a heat treated a 1/4” Cu tube into and S-shape to increase contact area (Fig. S2(a)), milling a channel in the shape of the tube into a Cu block (Fig. S2(b)), and soldering the Cu tube to the channel (Fig. S2(c, d)). The back side of the cold plate remained flat in order to hold the interdigitated comb device (Fig. S2(e)). The cold plate tube was then connected *via* a Swagelok compression fitting onto the stainless steel cooling water flow bellows tube lines (Fig. S3). Chilled water flows through the inlet bellows tube, along the inside of the cold plate and through the outlet. One support was used to hold the cold plate and the entire configuration in place.

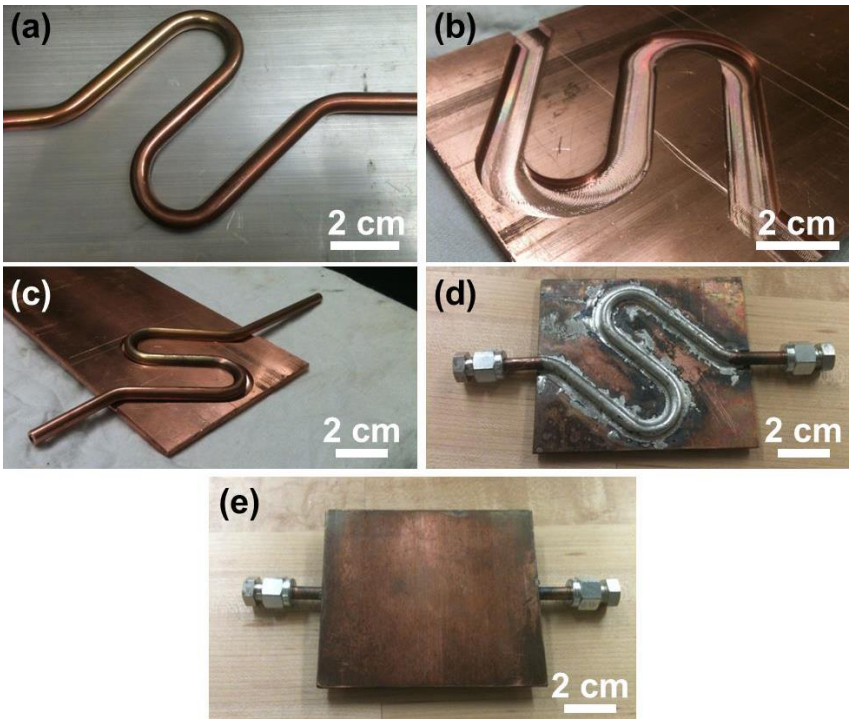

FIG. S2. Image of the cold-plate fabrication steps showing (a) 1/4" Cu heat treated tube after bending, (b) milled Cu cold plate block, (c) the tube resting in the milled cold plate block, (d) the cold plate after soldering, and (e) the cold plate front side (opposite of the soldering side).

S.3 CONDENSATION PROCEDURE

For each experimental run, a set of strict procedures were followed to ensure consistency throughout the experiments. The first step of the process was to turn on the voltage regulator to heat up the environmental chamber walls, which prevented condensation on the chamber walls. Simultaneously, the water vapor reservoir was filled with approximately 3.5 liters of DI water (99% full) using a syringe through the vapor release valve. After opening the vapor inflow valve and closing the vapor release valve, the rope heater around the water vapor reservoir was turned on with the heater controller set to maximum output (120 W). Then the rope heater connected to the vapor inflow valve was turned on. The temperature of the water reservoir was monitored with the installed thermocouples; the temperature at the top of the reservoir was higher than that of the middle/bottom of the reservoir due to the water thermal-mass present at the middle/bottom section. Hence, we ensured that the regions of the water reservoir of higher thermal capacity were brought to a sufficiently high temperature for boiling. During the boiling process, aluminum foil was placed on the bottom surface of the inner chamber to collect any of the water leaving the vapor inflow line. Once boiling was achieved and all thermocouples on the reservoir were >100˚C for at least 10 minutes, the vapor inflow valve was closed. The excess water that spilled inside the chamber during de-gassing of the reservoir was removed.

To install the cold plate onto the rig (Fig. S2), the Swagelok female adapters at the ends of the cold plate were connected to the 90 degree male elbow connecters on the rig. Before installing the cold plate in the chamber, all adapters/connecters were tightened to ensure that there were no leaks that could affect vacuum performance. The cold plate was then placed on top of the steel support and the bellows tubes (for the water inflow/outflow) were connected to the water lines (Fig. S3). After installation of the cold plate, the superhydrophobic CuO comb was placed on the cold plate surface with fins facing upwards and fin gaps aligned with the high speed camera viewport. To offset the hydrophilic Cu comb, four cylindrical Teflon spacers were placed at the four corners of the CuO comb (Fig. S3(b)). The Cu comb was placed on top of the spacers facing downward and aligning the fins to fit between the CuO fins and not make contact (interdigitating the two combs). The Teflon spacers not only electrically isolated the two combs, they acted as thermal insulation to ensure that only the CuO comb is cooled by the cold plate and avoid condensation on the Cu comb.

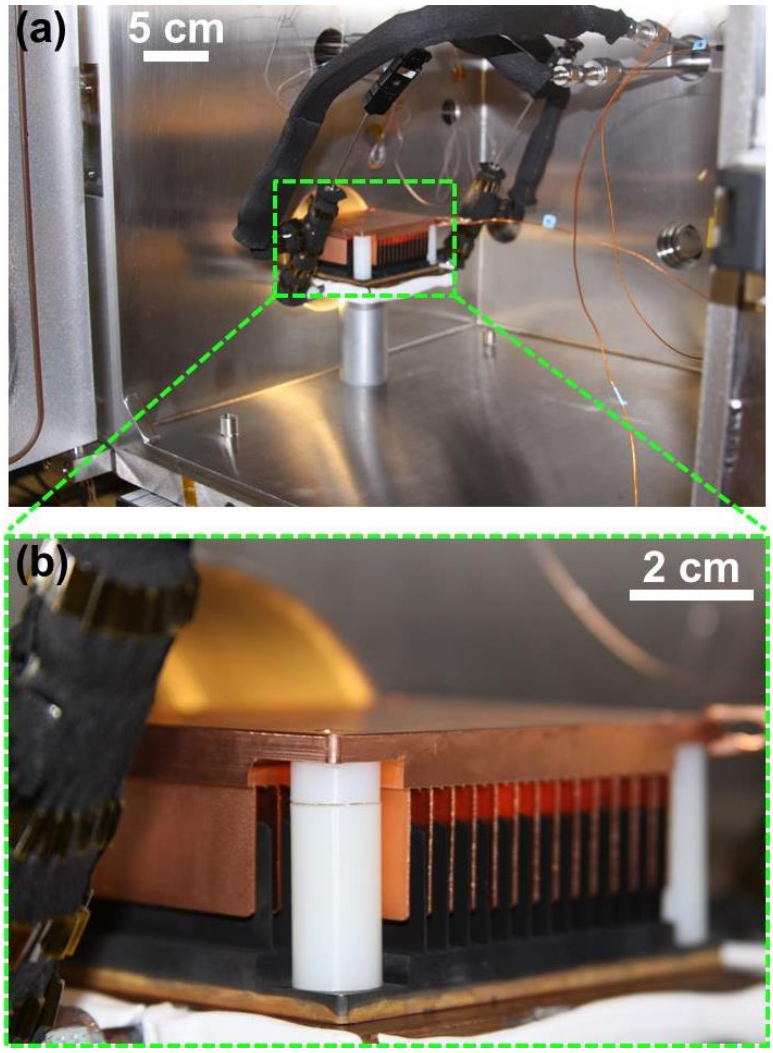

FIG. S3. (a) Image of the experimental setup inside the chamber with a (b) magnified view of the cold-plate showing the interdigitated CuO and Cu combs sitting on top. The base of the superhydrophobic CuO comb was in contact with the cold plate, while the hydrophilic Cu comb rested on top of the four Teflon spacers (white cylinders) and was electrically and thermally insulated from the CuO comb. To electrically insulate the CuO comb from the cold plate, Kapton tape was applied on top of the cold-plate surface.

Electrical Measurement Setup

To measure the electrostatic power potential of the interdigitated device, we measured the open circuit voltage (V_{OC}) and short circuit current (I_{CS}) during condensation. A high accuracy electrometer (6517B, Keithley Instruments) was electrically connected with a triaxial cable to the interdigitated combs *via* an electrical feed through (Kurt J. Lesker) mounted on a chamber aperture. Inside the chamber, the combs were connected to the electrical feed through *via*

insulated copper electrical wires. The electrometer was electrically connected (GPIB) to an analog input source (RAQ DAQ, National Instruments), which was interfaced to a computer for data recording.

Figures S4(a) and S4(b) show diagrams of the electrical connections used during the experiments to measure V_{OC} and I_{SC}, respectively. The chamber and electrometer chassis were grounded to the optical table. The chamber acted as both a ground and a shield for the electrical measurements.

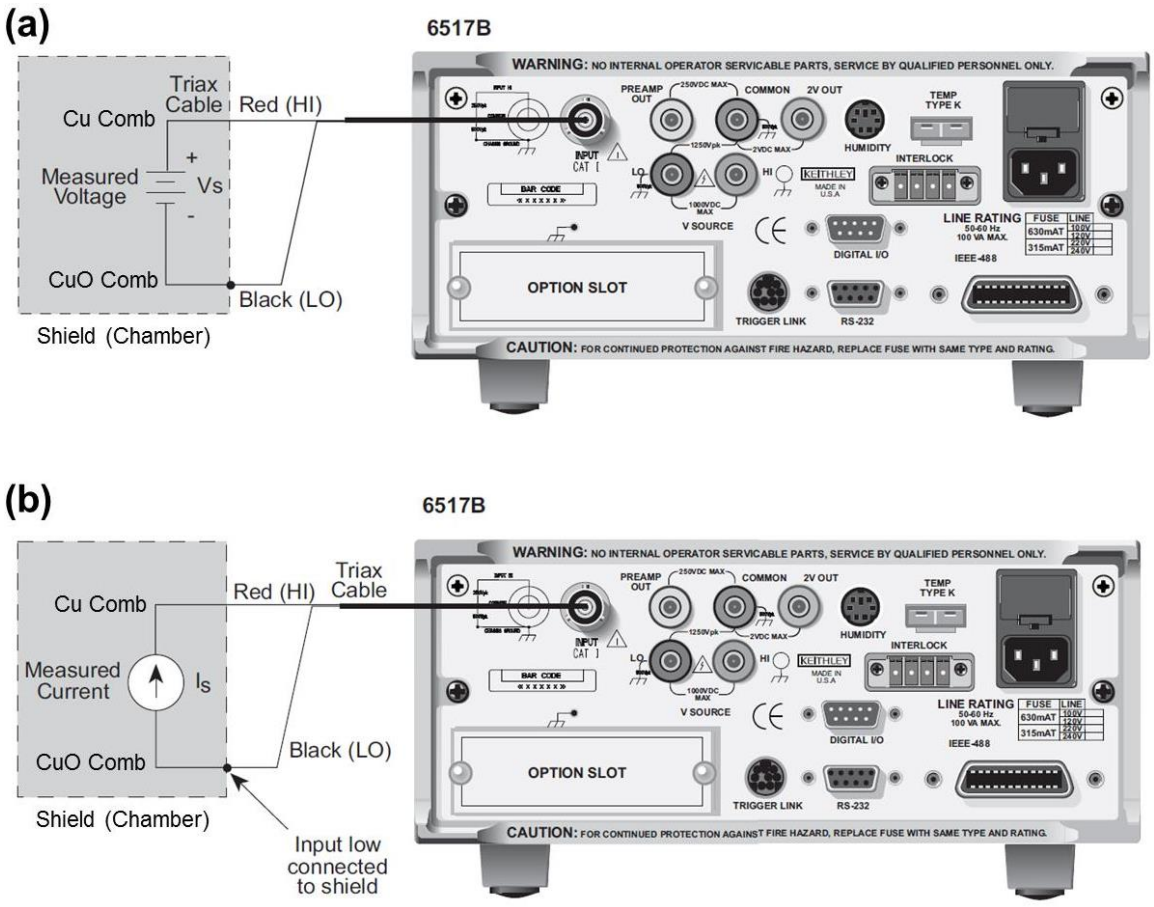

FIG. S4. Electrical circuit schematics of the (a) open circuit voltage, V_{OC} and (b) short circuit current, I_{SC}, measurement.[5] Adapted with permission from [5].

Condensation Procedure

Once the experimental setup was installed inside the chamber and the electrical connections (Fig. S4) were double checked for electrical shorts, the next step was to begin the vacuum pump-down procedure. Initially, the liquid nitrogen cold trap was filled to half capacity. The ambient exposed valves connecting the chamber and the vacuum pump were both closed and the valve connected to the liquid nitrogen cold trap was opened. The vacuum pump was then turned on, initiating the pump-down process. The pressure inside the chamber was monitored during the pump-down process. This process took approximately one hour in order to achieve the target vacuum conditions (0.5 Pa < P < 1 Pa). The experimental operating pressure of non-condensable was set to be a maximum of 0.25% of the operating pressure. In our experiments, extreme care was taken to properly de-gas the vacuum chamber and water vapor reservoir prior to experimental testing.

The setup of the water flow-loop is described as follows. The Neslab water pump reservoir was filled and turned on to a flow rate of 5 ± 0.25 L/min. The flow rate was monitored with the flow meter integrated in the inflow water line (0-5 L/min L-Series liquid flow meter, Alicat). In order to bring the chilled water into the flow loop and to the tube sample, the external chilled water lines were opened.

Prior to beginning the experiments, the high-speed camera was turned on for visual recording of the sample during condensation. Afterwards, the rope heater around the water reservoir was turned off and the vapor inflow valve was slowly turned open until the operating pressure was reached. Once the operating pressure was reached, the vapor inflow valve was closed and the vapor was allowed to reach thermal equilibrium inside the chamber. To initiate the condensation process for the short circuit measurement (Fig. S5), the chilled water supply temperature (T_c) was decreased ($t \approx 16$ minutes) until jumping droplet condensation was observed between the fins of the interdigitated device (Movies 1-3). During condensation, the vapor pressure (P_v) decreased due to the finite amount of vapor inside the chamber and T_c was maintained at ≈7.1°C. As the condensation process intensified due to transient cooling of the CuO fins, I_{SC} increased and eventually reached a quasi-steady value of $I_{SC} \approx 1.1 \pm 0.05$ nA ($t \approx 17.5$ minutes). After approximately 30 seconds of reaching a steady measurement, the cooling water temperature was increased ($t \approx 18$ minutes) and I_{SC} slowly decayed with time due to the smaller supersaturation

for condensation, and lower droplet jumping frequency. At $t \approx 22$ minutes, the chamber was vented *via* the bellows vent valve and condensation abruptly ended, resulting in the short circuit current decreasing rapidly to zero.

Note, during the short circuit test, T_c was lower than the saturation temperature at the water vapor pressure ($T_{sat}(P_v)$) in the chamber prior to condensation initiating ($t < 16$ minutes). This was due to the fin conduction resistance and temperature drop from the fin surface to the cooling water. In actuality, the fins surface was above $T_{sat}(P_v)$ until the cooling water temperature was lowered below 8°C.

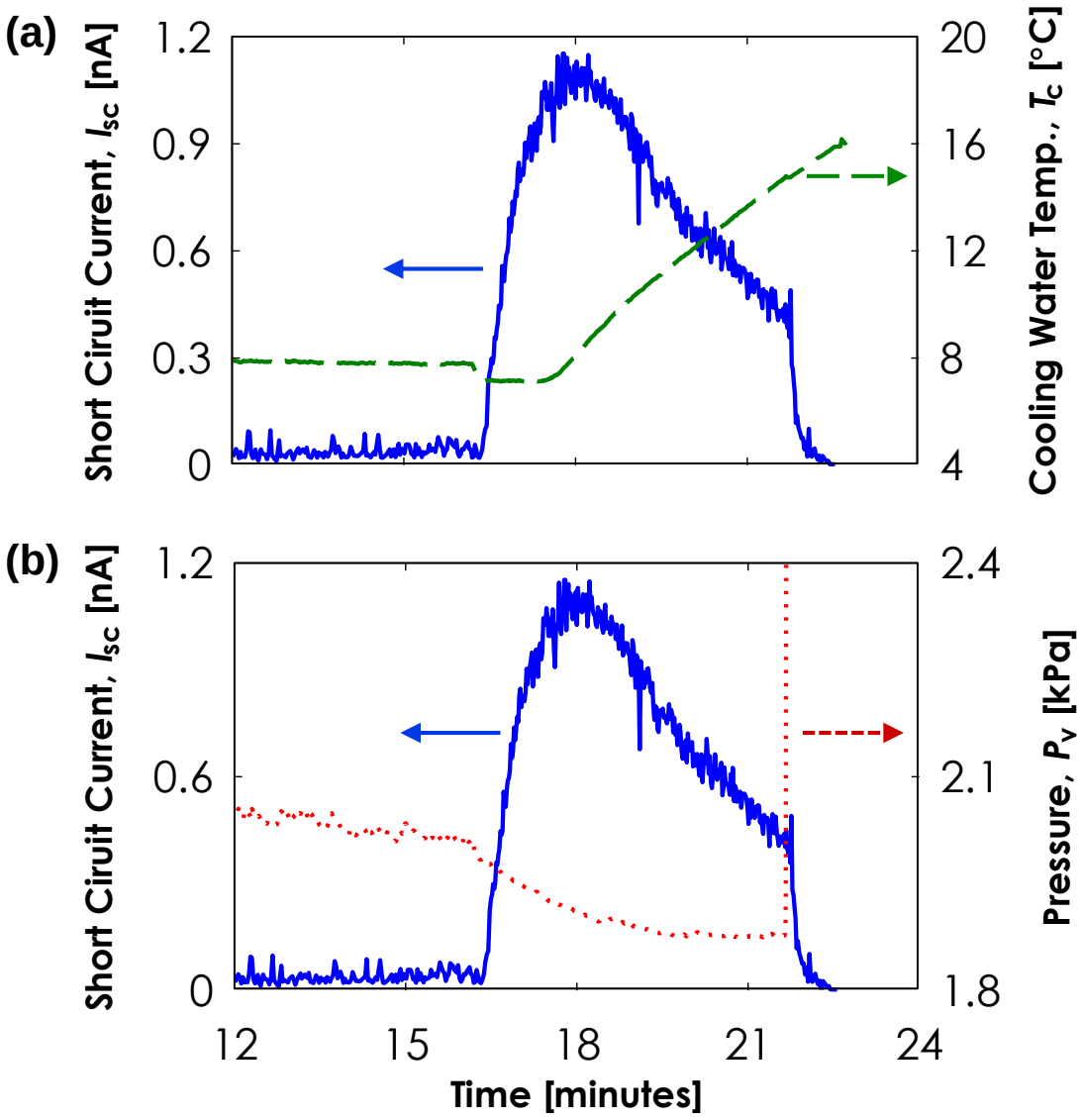

FIG. S5. Short circuit current (I_{SC}) measurement as a function of time (t) with (a) vapor pressure and (b) cooling water temperature overlaid.

References:

[1]N. Miljkovic, D. J. Preston, R. Enright, and E. N. Wang, ACS Nano **7** (12), 11043 (2013).
[2]N. Miljkovic, D. J. Preston, R. Enright, and E. N. Wang, arXiv:1310.2975 [physics.flu-dyn] (2013).
[3]K. Rykaczewski, A. T. Paxson, S. Anand, X. Chen, Z. Wang, and K. K. Varanasi, Langmuir **29** (3), 881 (2013).
[4]N. Miljkovic, R. Enright, Y. Nam, K. Lopez, N. Dou, J. Sack, and E. N. Wang, Nano Letters **13** (1), 179 (2013).
[5]Keithley Instruments, *Model 6517B Electrometer User's Manual*, 6517B-900-01 Rev. A / Jun 2008, 2008.